A preliminary results: study of crustal thickness in eastern part of Borneo, Indonesia from teleseismic receiver function analysis

Puji Ariyanto[1], *Imam* Tanthawi Anfasa[1*], *Marzuki* Sinambela[1], *Iman* Suardi[1], *Agus* Marsono[1], *Muhammad Adli* Dzilfikra[1], *Bayu* Pranata[2], *Relly* Margiono[3], and *Munawar* Ali[1]

[1]Department of Geophysics, State College of Meteorology Climatology and Geophysics, South Tangerang, Indonesia.
[2]Indonesian Agency for Meteorology Climatology and Geophysics, Jakarta, Indonesia.
[3]University of Adelaide, Adelaide, South Australia.

Abstract. The island of Borneo has relatively low seismic activity. However, the plan to relocate the capital city to the East Borneo region could potentially increase the population, making the area more vulnerable to earthquake occurrences. Therefore, this research aims to determine the depth of the Mohorovičić discontinuity layer, which will provide insights into the thickness of the Earth's crust, and model the local P and S wave velocities using the Inversion, Migration, and Stacking H-k methods. The data used consists of earthquake events with magnitudes greater than 6, located within a distance of 30° to 90° from 6 BMKG stations around the new capital of Indonesia. The research results indicate that the depth of the Mohorovičić discontinuity layer varies between 28 and 43 km. The model of P-wave velocities varies between 1.8 km/s to 9.1 km/s, while the model of S-wave velocities ranges from 1.0 km/s to 5.1 km/s.

1 Introduction

Indonesia is one of the countries consisting of many islands in the world. It is located at the intersection of three active tectonic plates, namely the Indo-Australian Plate, the Eurasian Plate, and the Pacific P late [1]. Borneo is part of the Sundaland region and is situated within the Eurasian continental plate [2]. One of the regions in Indonesia with the potential for earthquakes, albeit on a relatively small scale, is the island of Borneo. Borneo is the third-largest island in the world after Papua and Greenland. In its northern region, Borneo shares a direct border with Malaysia, while in the southern part, it is bordered by the Karimata Strait and the South China Sea, and in the eastern part, it is bordered by the Makassar Strait. Geologically, Borneo is located on the southeast side of the Eurasian Plate. To the north, the island is limited by the South China Sea Marginal Basin, to the east by the Makassar Strait, and to the south by the Java Sea. The eastern part of Borneo is characterized by several faults, including the Mangkalihat Fault, Sangkulirang Fault, and Peternoster Fault [3].

The Borneo region has a relatively low population density, accounting for only about 6% of Indonesia's total population [4]. The low population density is one of the reasons behind the enactment of Law Number (No.) 3 of 2022, which serves as the foundation for the construction of the State Capital in East Borneo [5]. Therefore, it is crucial to conduct disaster mitigation in the area, even though Borneo is considered relatively stable and experiences infrequent earthquakes (Figure. 1).

However, with the relocation of the capital to East Borneo, there is an anticipated increase in the population, and in the event of an earthquake, the impact could be more severe than before.

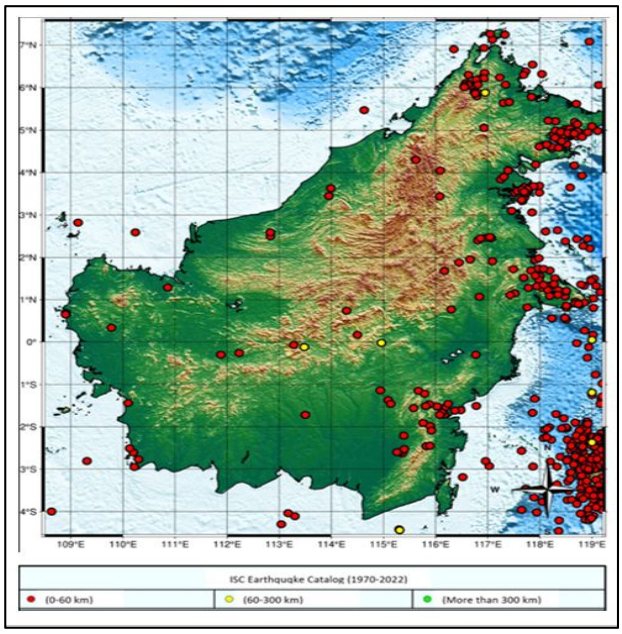

Fig. 1. Earthquake distribution map of Borneo Island from 1970 to 2022, based on ISC data.

* Corresponding author: imam.tanthawi.anfasa@stmkg.ac.id

This research aims to determine the thickness of the Earth's crust and analyze variations in P and S waves in the surrounding area of Indonesia's new capital city. Having an understanding of the Earth's crust thickness and the variations in P and S waves will prove immensely useful in validating the depths of hypocenters in the area surrounding the new capital city of Indonesia. This information will be of great significance to the Meteorology, Climatology, and Geophysics Agency (BMKG) as it enables them to provide fast and accurate data on hypocenter depth, which is vital for disaster mitigation efforts for the communities in the Capital City Region (IKN) located in Kutai Kertanegara and Penajam Paser, East Borneo. Receiver Function is a technique employed to gather data about the Earth's crustal structure using three-component seismic stations that record teleseismic waves. This method relies on the direct P-wave (P-wave), which converts into the S-wave (Ps converted wave) when it passes through certain layers of the Earth, such as the Mohorovičić discontinuity situated between the lower crust and upper mantle. By analyzing the time difference between the direct P-wave and the converted Ps-wave, researchers can estimate the depth of the Earth's crust [6]. To obtain information about the crustal structure, the horizontal component seismogram is deconvolved with respect to the vertical component. The purpose of this deconvolution process is to eliminate earthquake source and instrument response details [7].

Research using receiver function analysis has been increasingly conducted in Indonesia since 2002. The thickness of the transitional zone crust in Indonesia can be determined using the receiver function method with data from the Japan Indonesia Seismic Network [8]. This method is employed to calculate the depths of discontinuities at 410 km and 660 km, as well as to estimate the thickness of the mantle transition zone in Indonesia. The development of MATLAB scripts is used to calculate the depth of the Moho boundary. This is the result of collaboration between the Research and Development Center of BMKG and Gadjah Mada University [9]. Subsequently, research was conducted in the northern part of Sumatra and the Malay Peninsula using data from three BMKG seismograph networks, namely BSI, PSI, and GSI. The estimation results showed that the depth of the Moho layer is approximately 30-38 km, using a combined inversion of receiver function and phase velocity dispersion curves of surface waves to enhance the accuracy of the results [10]. The receiver function method is also utilized to estimate the thickness of sediment layers beneath East Borneo and East Java. Research in East Java indicated sediment layer thickness of about 1-4 km with an average Vs velocity of approximately 2.40 km/s, and crustal layer with an average Vs velocity of 4.70 km/s at a depth of 20 - 40 km. In East Borneo, the results revealed sediment thickness ranging from 5-10 km with an average Vs velocity of about 2.22 km/s, and the thickness of the Earth's crust varied between 34-50 km with an average Vs velocity of 4.48 km/s [11]. Furthermore, research in Borneo Island, divided into 5 zones - Sabah Zone, East Borneo Zone, Maratus Zone, Northwest Zone, and Southwest Zone, was conducted using nonlinear inversion methods. The results showed the thickness of sediment layers in Borneo Island varying from 1 to over 3 km. The thickest sediment layers were found beneath seismic stations located in the East Borneo region, with crustal thickness reaching 35 to 37 km and Vp/Vs velocity around 1.68 to 1.74 km/s [12].

This research presents a significant difference compared to some previous studies on Borneo Island. In this research, a seismic network consisting of 6 seismic stations distributed around the new capital city of Indonesia was used, and the area was divided into 3 provinces.: East Borneo, Central Borneo, and South Borneo. Additionally, the H-k Stacking method was also employed to analyze the data. It is expected that the results of this study, which provide information about the thickness of the Earth's crust and local models of P and S wave velocities beneath the stations, will enhance the accuracy in determining earthquake hypocenters. These findings are also anticipated to be valuable for other geophysical research.

2 Methodology

Receiver function is one of the methods that can be used to obtain information about the subsurface structure using three-component seismic stations and teleseismic waves, which are time-series functions that indicate the relative response of the Earth's structure beneath the receiving station. This response is generated by the propagation of seismic waves through media with different characteristics. When seismic waves propagate through a boundary plane, such as the Moho Discontinuity, transmission, refraction, conversion, and reflection processes occur, depending on the material properties of the boundary and the angle of wave incidence.

The Moho Discontinuity serves as an example of such a boundary plane. P waves passing through the boundary (Moho) will be transmitted and identified as the Pp phase by the receiving station. And P waves that are converted into S waves are identified as the Ps phase by the receiving station. The arrival time of the Ps wave will be slower than the direct P wave (Pp) due to the velocity difference between the slower S wave and the P wave. The time difference between the Pp and Ps phases can be used to determine the crustal thickness by examining the depth of the Moho Discontinuity beneath the receiving station, provided that the local velocity model is also known. In addition to the conversion process, reflection and refraction processes of the waves also occur. Reflected waves that return to the mantle as P waves and S waves are not required in the receiver function analysis process. The reflected waves used are those that are reflected between the upper crust and the air (free surface), then reflected back and converted by the Moho Discontinuity, resulting in multiple phases (PpSs+PsPs and PpPs) recorded by the receiving station. The PpSs phase results from the direct refraction of P waves, which become P waves again after reflection from the free surface, then further reflected as S waves. The PsPs phase results from the refraction of P waves, which are converted into S waves and then reflected by the free surface, becoming P waves again and then reflected back as S waves. The PpPs phase results from the direct refraction of P waves,

becoming P waves again after reflection from the free surface, and upon encountering the Moho Discontinuity, being converted into S waves (Figure. 2).

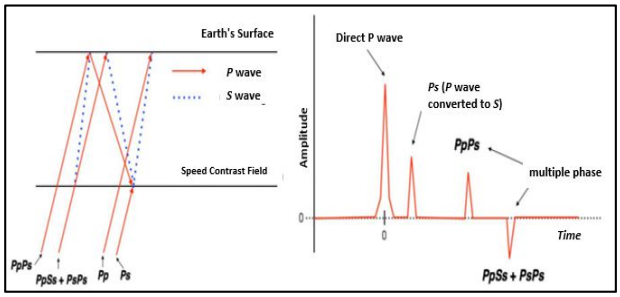

Fig. 2. Receiver function diagram. Ps conversion phase and reflection phases (PpPs and PpSs+PsPs) translated from a simple Earth layer model [13] The Figure is modified by [14, 15].

2.1 Rotation

The original coordinate system of teleseismic waveforms is ZNE (Vertical, North-South, and East-West coordinates). The ZNE coordinate system has the propagation direction of earthquake sources not aligned with the receiving station. Therefore, it is necessary to rotate the horizontal N (North-South) component into the radial (R) component and the E (East-West) component into the tangential (T) component. This is done to align the seismogram signal with the direction of the seismic waves' arrival and to make the received wave phases clearer. To perform the rotation process, the ZNE components are transformed into ZRT (vertical, radial, and tangential) components:

$$\begin{bmatrix} R \\ T \\ Z \end{bmatrix} = \begin{bmatrix} -Cos\,\gamma & -Sin\,\gamma & 0 \\ Sin\,\gamma & -Cos\,\gamma & 0 \\ 0 & 0 & 1 \end{bmatrix} \begin{bmatrix} N \\ E \\ Z \end{bmatrix} \quad (1)$$

Where the horizontal components (NE) are rotated into the radial (R) component, aligned with the direction of wave arrival, the tangential (T) component is perpendicular to the wave's arrival direction, the vertical component (Z) remains unchanged, and γ represents the back azimuth, indicating the direction of teleseismic wave arrival from the north of the station coordinates.

2.2 Iterative time domain deconvolution

Iterative Time Domain Deconvolution utilizes a forward modeling approach, where an iterative convolution process of several wavelet models, $Ei(t)$, takes place. Here, $E(t)$ represents the response of the local structure determined from the signal model with the minimum misfit between the convolution results of synthetic seismogram signals and observed signals. Then, $Z(t)$ represents the vertical component seismogram to obtain the radial and tangential component signals. The equations are as follows:

$$\begin{aligned} T\,(t) &= EiT\,(t) * Z(t) \\ R\,(t) &= EiR\,(t) * Z(t) \end{aligned} \quad (2)$$

Where $T(t)$ and $R(t)$ are the tangential and radial component seismograms in the time domain, and $EiT(t)$ and $EiR(t)$ are the respective iterative model receiver functions for the tangential and radial components, obtained iteratively. * denotes the convolution operator, and then $Z(t)$ is the vertical component seismogram. The value of $ET(t)$ will be equivalent to $EiT(t)$ if the misfit between $R(t)$ and the convolution of $EiR(t)$ with $Z(t)$ is minimized. In this study, a fit criterion of over 90% is used.

To find the value of $Ei(t)$, a low-pass Gaussian filter is employed, which is useful for isolating wave signals at low frequencies and eliminating high-frequency noise. The calculation can be expressed as follows:

$$G\,(\omega) = exp\,(\frac{-\omega}{4a^2}) \quad (3)$$

Where ω is the gain of the Gaussian filter, and at $\omega = 0$, it equals one (unit pulse area). α is the parameter controlling the width of the Gaussian filter's frequency, and its value varies from 0.5 to 2.0. In this research, a value of $\alpha = 1.5$ is used as it provides the best estimate for the receiver function [13]. Then, the estimation of the receiver function is convoluted with the vertical component and subsequently subtracted from the radial component iteratively, which is useful for estimating the time-amplitude differences and peak-to-peak differences of a receiver function. When the iteration reaches the minimum misfit value, the iteration process stops.

2.3 Inversion

The inversion is conducted to obtain a suitable match between the calculated data and the observed data by employing forward modeling until the smallest fitting is achieved, resulting in a velocity model of the subsurface beneath the receiver station [15]. Then, an initial model is provided, using the global velocity model AK-135 [16]. This is done using the equation:

$$y = F\,[x] \quad (4)$$

Where y is an n-dimensional vector of data points, $F[\ ]$ is a nonlinear operator that transforms the model vector into a vector with the same domain as the y-domain. x is an m-dimensional vector representing S-wave velocities at various depths of lithospheric layers, describing the model. The nonlinear equation is then iteratively inverted using linearization as follows:

$$\begin{aligned} \delta y &= \nabla F\,|xn\,.\,\delta xn \\ Xn + 1 &= xn + \delta xn \end{aligned} \quad (5)$$

Where $\delta y = y - F[xn]$ is the data residual vector, and $\delta xn = xn - x$ is the model correction vector.

2.4 Migration of AK-135 velocity model

Migration can eliminate diffraction effects, thus providing a clearer image of subsurface structural details. This process aims to map seismic events at their actual positions by relocating data elements from the midpoint locations to subsurface point locations [17].

In receiver function migration, the significant station is selected, and the time domain is transformed into the signal domain, which is then converted into the depth domain to determine the points of wave conversion appearance. This is done with the help of an existing velocity model, such as the global velocity model AK-135. The conversion points from the propagation paths are accumulated to obtain a projection model. Then, the discontinuity layers are determined by stacking the seismic energy distribution from each event. The advantage of this migration process is particularly useful in areas with lateral velocity variations, which tend to be complex regions. The equation to convert from the time domain to the depth domain is as follows:

$$H = \frac{Tps}{\sqrt{\frac{1}{vs2} - p2} - \sqrt{\frac{1}{vp2} - p2}} \quad (6)$$

H represents depth, Tps is the travel time of Ps wave conversion, p is slowness, Vs is the S-wave velocity, and Vp is the P-wave velocity.The inversion is conducted to obtain a suitable match.

2.5 Stacking H-k

Stacking H-k method is one of the techniques that can be used to determine the average Vp/Vs ratio (k) and estimate the structure and composition of the Earth's crust. This is achieved by calculating the arrival times of different wave phases, such as Ps, PpPs, and PpSs+PsPs, with respect to the direct P wave [6]. The advantage of this method is that it simplifies waveform processing for a significant number of teleseismic earthquakes. Additionally, it eliminates the need for picking different conversion waves, allowing the retrieval of crustal thickness models from different directions when their values are at their maximum.

The equations for the time differences of wave arrivals are as follows, where t1 represents the equation for the Ps wave, t2 for the PpPs wave, and t3 for the PpSs+PsPs wave:

$$t1\,[H,K] = H\left[\sqrt{\frac{K2}{vp2} - p2} - \sqrt{\frac{1}{vp2} - p2}\right]$$
$$t2\,[H,k] = H\left[\sqrt{\frac{K2}{vp2} - p2} + \sqrt{\frac{1}{vp2} - p2}\right]$$
$$t3\,[H,k] = 2H\sqrt{\frac{K2}{vp2} - p2} \quad (7)$$

Where Vp is the velocity of the P wave (s/km), and p is the value of slowness (s/km). Subsequently, the following equation is used for H-k stacking to estimate the thickness of the Earth's crust:

$$s\,(H,k) = \sum_{j=1}^{N} w\,1\,rj\,(t1\,[H,k]) + w2rj\,(t2[H,k]) - w3rj\,(t3\,[H,k]) \quad (8)$$

When the Ps, PpPs, and PpSs+PsPs wave phases show maximum coherence during stacking, the value of s (H, κ) will be high and reflect the actual values of H and κ.

3 Data and processing

3.1 Data

The research data used in this study consists of teleseismic earthquake waveform data recorded by six seismic sensor networks of BMKG. This seismic sensor is a three-component seismometer located in three provinces surrounding the new capital city of Indonesia, with coordinates boundaries in this study ranging from 4° S to 7° N and 114.5° to 118° E (Figure. 3).

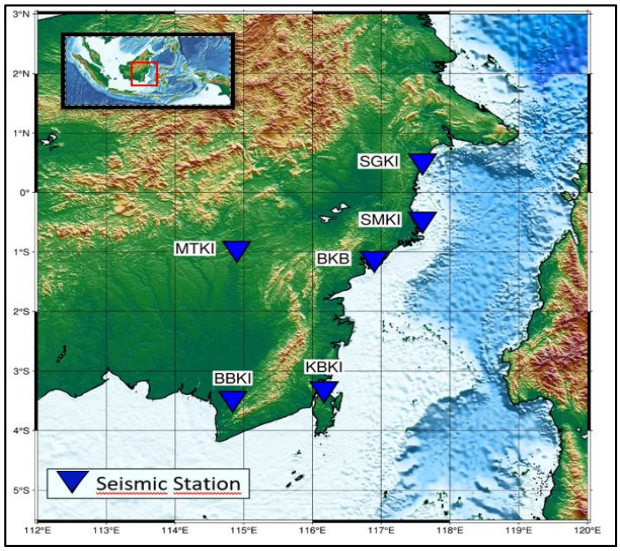

Fig. 3. Map of the distribution of Seismic Sensors.

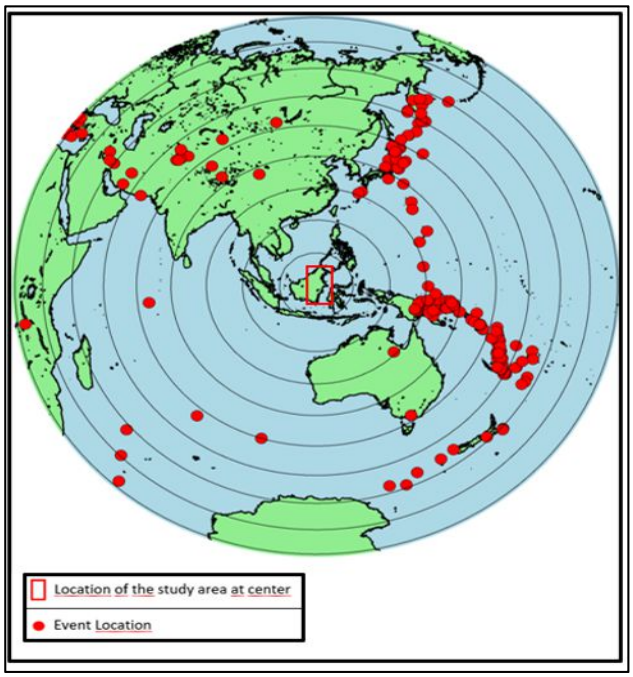

Fig. 4. The distribution of Teleseismic Earthquakes.

The data used includes P-wave teleseismic recordings with a magnitude of M ≥ 6 and a distance of 30° to 90° from the research sensors (Figure. 4). The data was downloaded through the BMKG and Incorporated Research Institutions for Seismology (IRIS) websites in mseed format. The coordinates of the seismic sensors and the distribution map of the stations to be used in this study are shown in (Figure. 4).

3.2 Processing

The data processing method is carried out in several stages. The first stage is the selection of teleseismic earthquake data based on predetermined criteria. Seismic wave data is collected within a time range of 20 minutes before the P-wave phase and 20 minutes after the S-wave phase. The data in mseed format is then converted into fullseed format with additional instrument response parameters. The fullseed data is then extracted into SAC format using rdseed software. From the obtained seismograms, recordings with a high signal-to-noise ratio (SNR) and clear initial P-wave phase are manually selected. In the processing of teleseismic signals, CPS (Computer Programs in Seismology) software developed by [18] is used. Next, the seismograms undergo baseline correction by subtracting their mean values. To isolate the Ps conversion phase, the North-South (NS) and East-West (EW) components of the seismograms are rotated into radial and tangential components. Then, the receiver function is calculated for the radial and tangential components using an iterative time-domain deconvolution method with 500 iterations, following the technique developed by [13]. The receiver function calculation results that have a fit criterion of 90% or higher compared to the observed receiver function will be used for further analysis. The receiver function signals on the radial component obtained from the deconvolution process are then mapped as a function of back azimuth against time to identify crustal structures based on wave phases.

To identify the depth of layers and illustrate strong complex structures, the receiver function signals are further migrated from the time domain to the depth domain using the global velocity model AK-135. Finally, as validation of several previous methods, the last method used is H-k stacking.

4 Result and discussion

The Receiver Function analysis was conducted at 6 BMKG seismic stations to understand the thickness of the Earth's crust in the area surrounding Indonesia's new capital city. This area includes three provinces: East Borneo, Central Borneo, and South Borneo.

4.1 East borneo province

In the East Borneo province, there are three stations: Sangatta Station (SGKI), Samarinda Station (SMKI), and Balikpapan Station (BKB). SGKI Station is located at coordinates 0.53° S and 117.6° E in the Sangatta area of East Borneo. Using 55 receiver functions, the results of plotting fifty-five radial component receiver functions based on back azimuth and the stacking results can be seen in (Figure. 5). The Ps conversion phase is evident at around 5.5 seconds. SMKI Station is situated at Latitude -0.45 and Longitude 117.21° in the Samarinda area. Utilizing 57 receiver functions, the results of plotting fifty-seven radial component receiver functions based on back azimuth and the stacking results are shown in (Figure. 6). The Ps conversion phase is visible at around 4 seconds. BKB Station is located at Latitude -1.26 and Longitude 116.89° in the Balikpapan area. Using 77 receiver functions, the results of plotting seventy-seven radial component receiver functions based on back azimuth and the stacking results are displayed in (Figure. 7). The Ps conversion phase is observed at around 5.9 seconds.

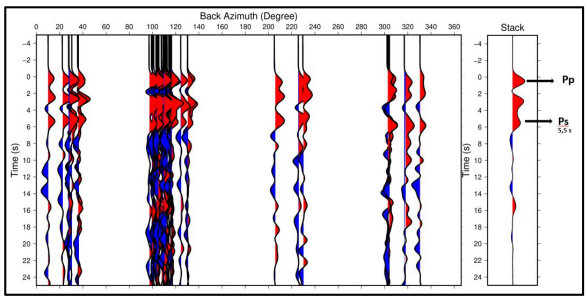

Fig. 5. Receiver function and stacking at SGKI Station plotted based on back azimuth.

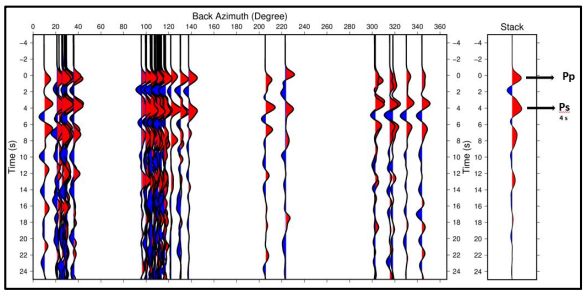

Fig. 6. Receiver function and stacking at SMKI Station plotted based on back azimuth.

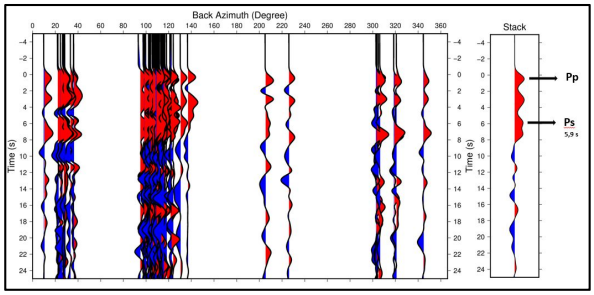

Fig. 7. Receiver function and stacking at BKB Station plotted based on back azimuth.

The velocity structure of P and S waves is depicted through the inversion results of the receiver function at SGKI station. The inverted signals are obtained from the stacking process, showing an 89.08% match between the inverted signals and the observations below the SGKI station. (Figure. 8) illustrates the comparison between the inverted signals and the observations. (Figure. 9) displays the profile of P-wave velocity below the SGKI station. The velocity range of P-waves from the surface to a depth of 100 km is between 3.7 km/s and 9.1 km/s, with minimum and maximum values. At depths of 2 - 6 km, the velocity range is approximately 3.0 - 4.5 km/s. Then, at depths of 7 - 10 km, the velocity becomes around 4.3 - 4.4 km/s. Subsequently, it increases significantly, reaching a value of 10.2 km/s at a depth of 46 km. The significant increase in wave velocity is associated with the depth of the Moho discontinuity. This phenomenon is caused by the denser material in the Earth's mantle compared to the

Earth's crust. Based on the P-wave velocity profile, the depth of the Moho discontinuity layer beneath the SGKI station is estimated to be within the depth range of 30 - 34 km, with P-wave velocities in the crust ranging from 3.0 - 7.7 km/s. (Fig. 10) presents the profile of S-wave velocity below the SGKI station. The velocity range of S-waves from the surface to a depth of 100 km is between 1.7 km/s and 5.7 km/s, with minimum and maximum values. At depths of 2 - 6 km, the velocity range is approximately 1.7 - 2.5 km/s. Then, at depths of 7 - 10 km, the velocity becomes around 2.3 - 2.4 km/s. Subsequently, it increases significantly, reaching a value of 4.3 km/s at a depth of 30 km. According to the inversion results, S-wave velocities in the crust are valued between 1.7 - 3.2 km/s.

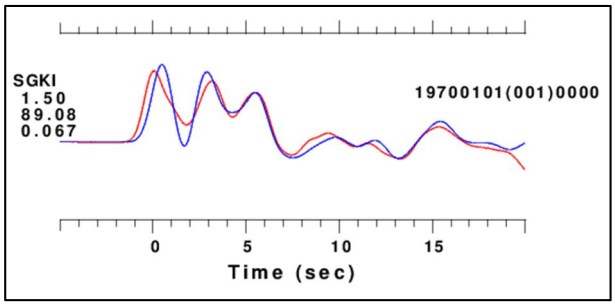

Fig. 8. Comparison of inversion results (red) and observations (blue) from receiver function stacking signals at SGKI Station.

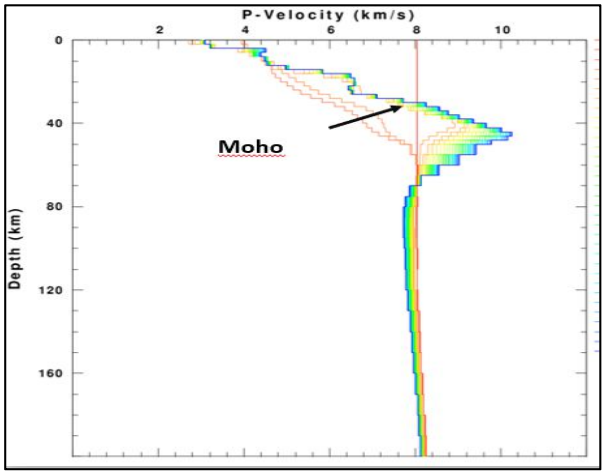

Fig. 9. Profile of P-wave velocity at SGKI Station.

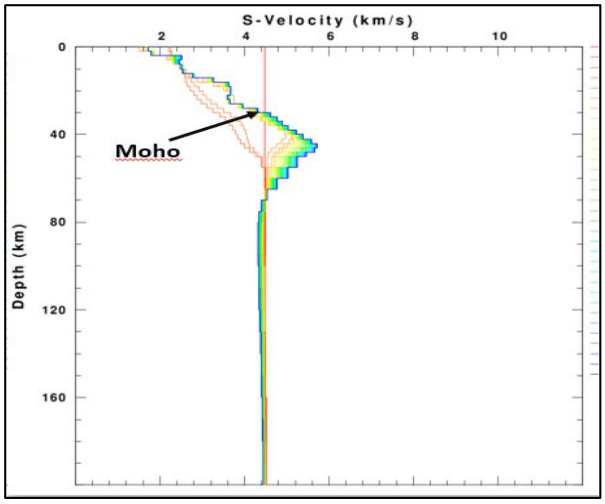

Fig. 10. Profile of S-wave velocity at SGKI Station.

The velocity structure of P and S waves is depicted through the inversion results of receiver functions at the SMKI station. The inverted signals are obtained from the stacking process, showing an 85.35% match between the inverted signals and observations beneath the SMKI station. (Figure. 11) illustrates the comparison between the inversion results and observations. (Figure. 12) presents the profile of P-wave velocity beneath the SMKI station. In the range from the surface to a depth of 10 km, the velocity changes from 3.7 km/s to 5.6 km/s. Then, at depths of 11 - 20 km, the velocity decreases from 3.9 km/s to 4.7 km/s. Subsequently, at depths of 21 - 34 km, there is an increase from 6.0 km/s to 7.7 km/s. At a depth of 34 km, there is a significant increase, reaching its maximum value at a depth of 65 km, where the maximum P-wave velocity is 9.1 km/s. The significant increase in wave velocity is related to the depth of the Moho discontinuity. This phenomenon is caused by the denser material in the Earth's mantle compared to the Earth's crust. Based on the P-wave velocity profile, the depth of the Moho discontinuity beneath the SMKI station is estimated to be between 28 - 30 km, with P-wave velocities in the crust ranging from 3.7 – 7.7 km/s. (Fig. 13) displays the profile of S-wave velocity beneath the SMKI station. The range of S-wave velocities from the surface to a depth of 100 km is between 2.0 km/s and 5.1 km/s, with minimum and maximum values. At depths of 2-10 km, the velocity changes from 2.0 km/s to 3.1 km/s. Then, at depths of 11 - 20 km, the velocity decreases from 2.1 km/s to 2.6 km/s. Subsequently, at depths of 21 - 34 km, there is an increase from 3.3 km/s to 4.3 km/s. At a depth of 34 km, there is a significant increase, reaching its maximum value at a depth of 65 km, where the maximum S-wave velocity is 5.1 km/s. Based on the inversion results, S-wave velocities in the crust range from 2.0 – 4.3 km/s.

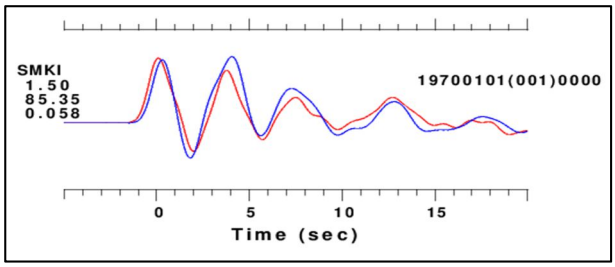

Fig. 11. Comparison of inversion results (red) and observations (blue) from receiver function stacking signals at SMKI Station.

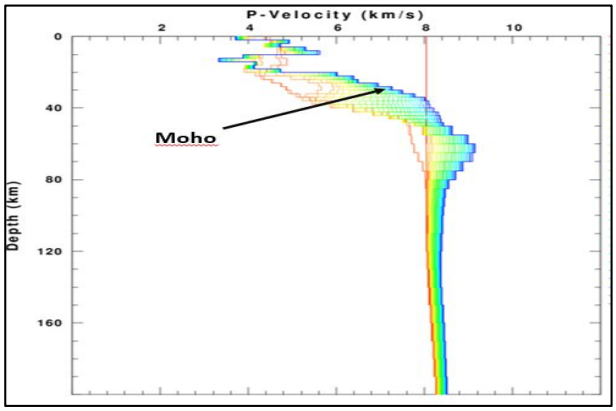

Fig. 12. Profile of P-wave velocity at SMKI Station.

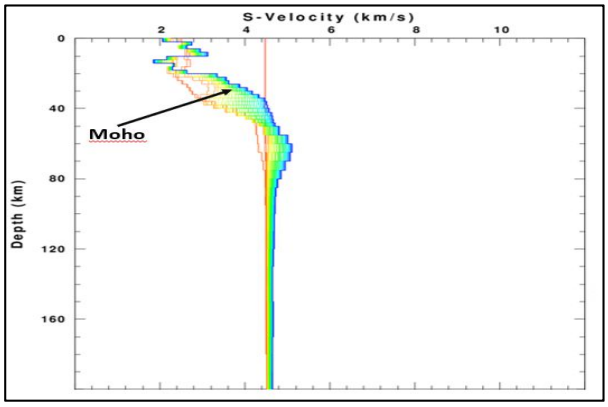

Fig. 13. Profile of S-wave velocity at SMKI Station.

The velocity structure of P and S waves is depicted through the inversion results of the receiver function at BKB station. The inverted signals are obtained from the stacking process. There is a matching percentage of 90.67% between the inverted signals and observations beneath the BKB station. (Fig. 14) shows the comparison between the inverted signals and observations. (Figure. 15) presents the profile of P-wave velocity beneath the BKB station. The velocity range of P waves from the surface to a depth of 100 km is between 1.8 km/s and 9.8 km/s, with minimum and maximum values. From the surface to a depth of 20 km, the velocity range is approximately 1.8 km/s to 6.2 km/s. Then, at a depth of 21 – 24 km, the P-wave velocity decreases to 5.7 – 5.8 km/s. At a depth of 25 - 31 km, the P-wave velocity increases to 6.6 – 7.2 km/s. Subsequently, at a depth of 32 - 55 km, there is a significant increase in P-wave velocity to 6.7 - 9.8 km/s. The significant increase in wave velocity is associated with the depth of the Moho discontinuity. This phenomenon is caused by the denser material in the Earth's mantle compared to the Earth's crust. Based on the P-wave velocity profile, the depth of the Moho discontinuity beneath the BKB station is estimated to be between 32 - 36 km, with the P-wave velocity in the crust ranging from 1.8 – 7.7 km/s. (Fig. 16) displays the profile of S-wave velocity beneath the BKB station. The velocity range of S waves from the surface to a depth of 100 km is between 1.0 km/s and 5.4 km/s, with minimum and maximum values. From the surface to a depth of 20 km, the velocity range is approximately 1.0 km/s to 3.4 km/s. Then, at a depth of 21 – 24 km, the S-wave velocity decreases to 3.1 – 3.2 km/s. At a depth of 25 - 31 km, the S-wave velocity increases to 3.6 – 4.0 km/s. Subsequently, at a depth of 32 - 55 km, there is a significant increase in S-wave velocity to 3.7 – 5.4 km/s. Based on the inversion results, the S-wave velocity in the crust is estimated to be between 1.0 – 4.3 km/s.

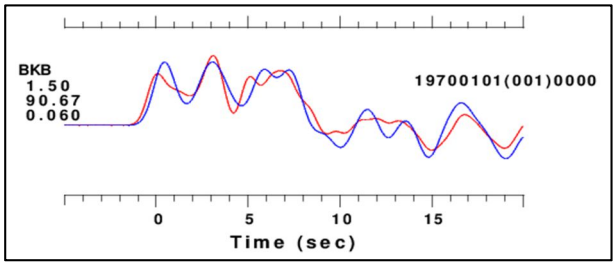

Fig. 14. Comparison of inversion results (red) and observations (blue) from receiver function stacking signals at BKB Station.

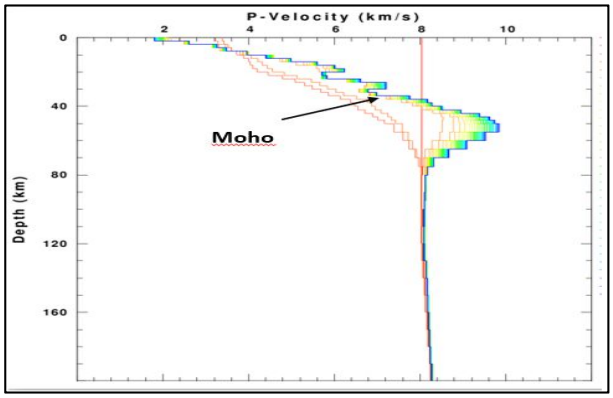

Fig. 15. Profile of P-wave velocity at BKB Station.

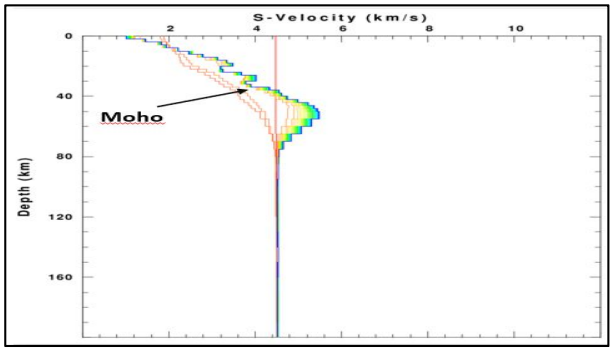

Fig. 16. Profile of S-wave velocity at BKB Station.

Next, to obtain the depth using Migration, the AK-135 velocity model is used to migrate the receiver function from the time domain to the depth domain. The migration results using the AK-135 velocity model show that the depth of the Mohorovicic Discontinuity layer beneath SGKI Station is approximately 40 km (Figure. 17). Meanwhile, SMKI Station is located at a depth of around 33 km (Fig. 18), and BKB Station is situated at a depth of approximately 46 km (Figure. 19).

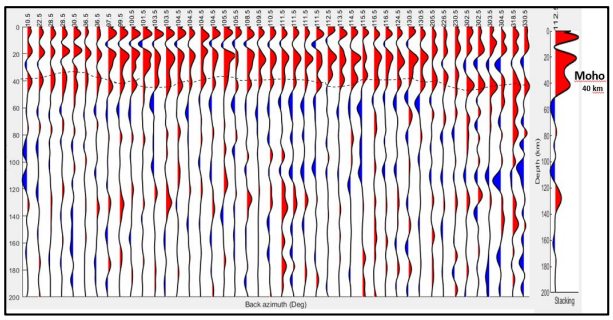

Fig. 17. The migration results using the AK-135 velocity model at SGKI Station.

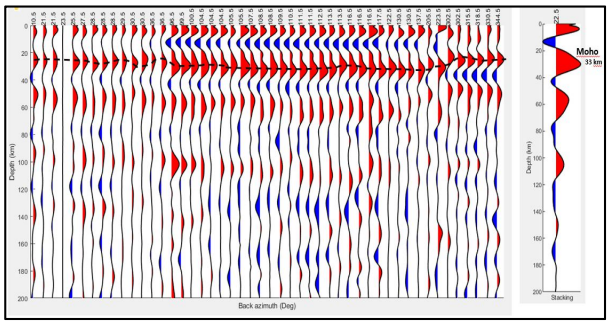

Fig. 18. The migration results using the AK-135 velocity model at SMKI Station.

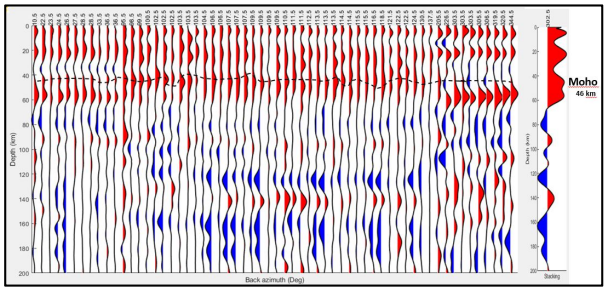

Fig. 19. The migration results using the AK-135 velocity model at BKB Station.

Lastly, to obtain the depth and Vp/Vs velocity values, the H-k Stacking method was utilized using the Matlab application. The analysis results showed that the depth of the Mohorovičić Discontinuity layer at SGKI Station is approximately 34.39 km, with a Vp/Vs velocity of 1.96 km/s (Figure. 20). At SMKI Station, the Moho layer was found at a depth of around 30.25 km, with a Vp/Vs velocity of 1.81 km/s (Figure. 21). Meanwhile, at BKB Station, the Moho layer was at a depth of about 36.6 km, with a Vp/Vs velocity value of 1.97 km/s (Figure. 22).

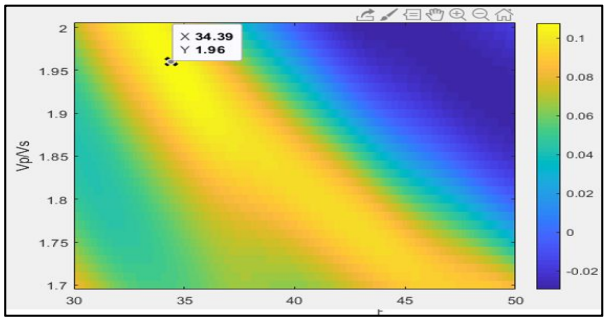

Fig. 20. The results of Moho depth and Vp/Vs velocity using Stacking H-k at SGKI Stations.

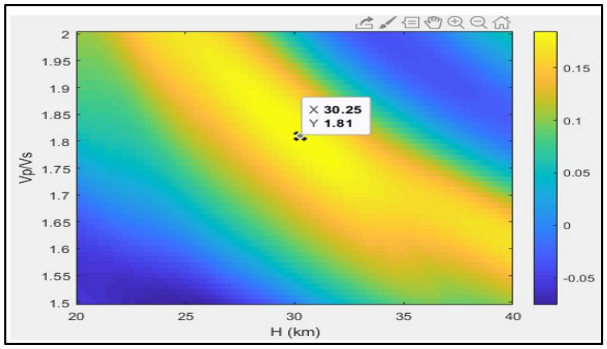

Fig. 21. The results of Moho depth and Vp/Vs velocity using Stacking H-k at SMKI Stations.

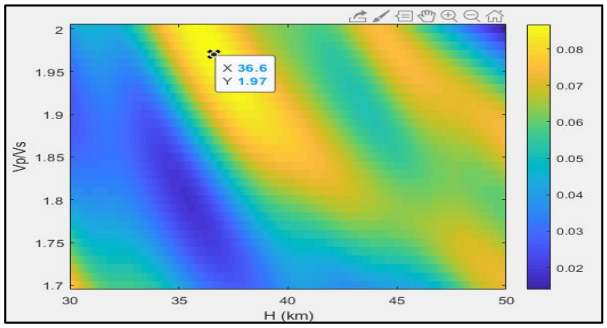

Fig. 22. The results of Moho depth and Vp/Vs velocity using Stacking H-k at BKB Stations.

4.2 Central Borneo Province

In the Central Borneo province, there is a seismic station called Muara Taweh Station (MTKI) located at the geographic coordinates of Latitude -0.94 and Longitude 114.89. In this study, 65 receiver functions were used with a criteria of fit values ≥ 90%. The results of plotting sixty-five radial component receiver functions based on back azimuth and the stacking results can be seen in (Figure. 23). In the plot, the Ps conversion phase can be observed occurring at approximately ~ 4.3 seconds.

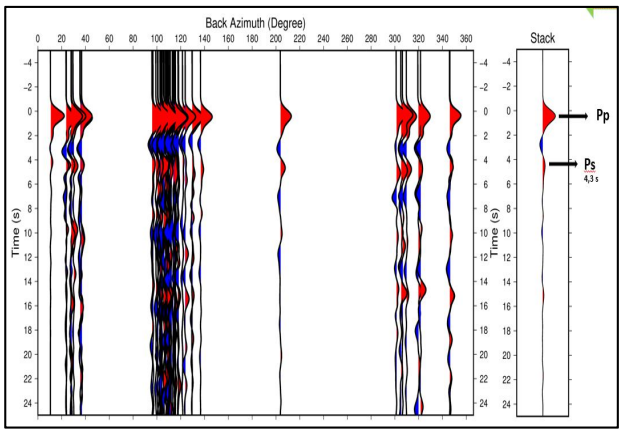

Fig. 23. Receiver function and stacking at MTKI Station plotted based on back azimuth.

The velocity structure of P and S waves is shown through the inversion results of the receiver function at station MTKI. The inverted signals are the outcome of the stacking process, showing a matching level of 95.49% between the inverted signals and observations beneath station MTKI. The comparison between the inverted signals and observations is displayed in (Figure. 24). Displays the profile of P-wave velocity beneath station MTKI (Figure. 25). The velocity range of P waves from the surface to a depth of 100 km is between 3.7 km/s to 9.2 km/s. From the surface to a depth of 14 km, the velocity increases to approximately 3.7 km/s to 7.1 km/s. Then, at depths of 15 - 26 km, there is a decrease in velocity to around 6.7 km/s to 6.9 km/s. At depths of 27 - 60 km, the velocity significantly increases to approximately 7.2 km/s to 9.2 km/s. This significant velocity increase is associated with the depth of the Moho discontinuity. This phenomenon is caused by the presence of denser material in the Earth's mantle compared to the Earth's crust. Based on the P-wave velocity profile, the estimated depth of the Moho discontinuity beneath station MTKI is around 32 - 36 km, with P-wave velocity in the Earth's crust ranging between 3.7 km/s to 8.0 km/s. (Fig. 26) displays the profile of S-wave velocity beneath station MTKI. The velocity range of S waves from the surface to a depth of 100 km is between 2.0 km/s to 5.2 km/s. From the surface to a depth of 14 km, the velocity increases to approximately 2.0 km/s to 3.9 km/s. Then, at depths of 15 - 26 km, there is a decrease in velocity to around 3.7 km/s to 3.8 km/s. At depths of 27 - 60 km, the velocity significantly increases to approximately 4.0 km/s to 5.1 km/s. Based on the velocity profile, S-wave velocity in the Earth's crust is identified to be between 2.0 km/s to 4.4 km/s.

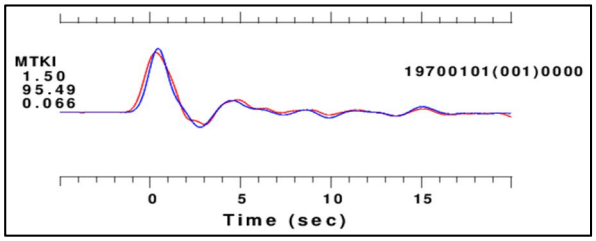

Fig. 24. Comparison of inversion results (red) and observations (blue) from receiver function stacking signals at MTKI Station.

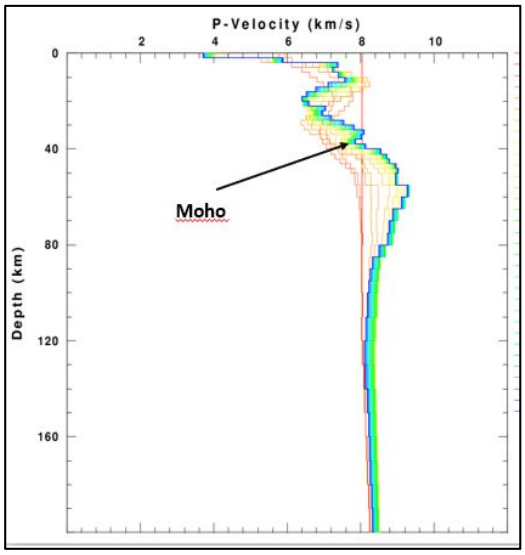

Fig. 25. Profile of P-wave velocity at MTKI Station.

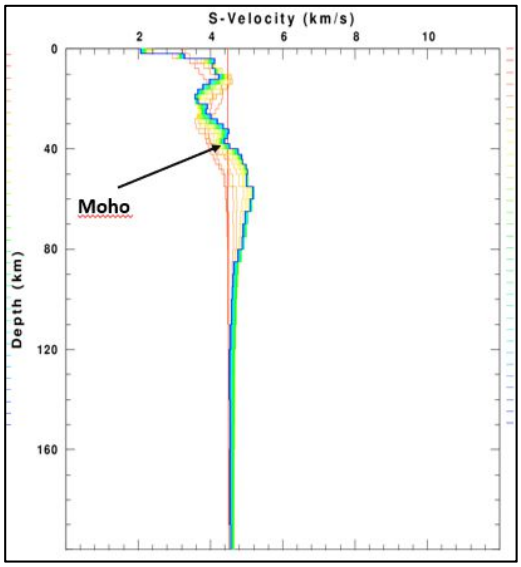

Fig. 26. Profile of S-wave velocity at MTKI Station.

Next, the migration results using the AK-135 velocity model revealed a depth of approximately ~33 km for the Mohorovicic Discontinuity layer (Figure. 27). Finally, the results of the H-k Stacking method indicated a depth of approximately ~36.34 km for the Mohorovicic Discontinuity layer, with a Vp/Vs velocity ratio of 1.75 km/s (Figure. 28).

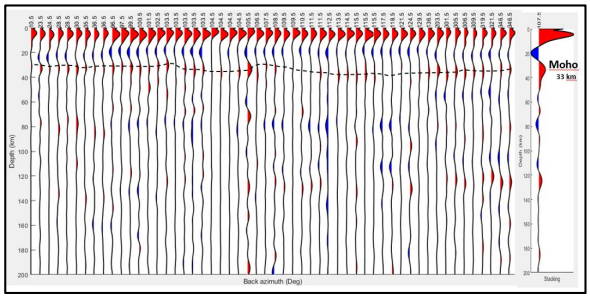

Fig. 27. The migration results using the AK-135 velocity model at MTKI Station.

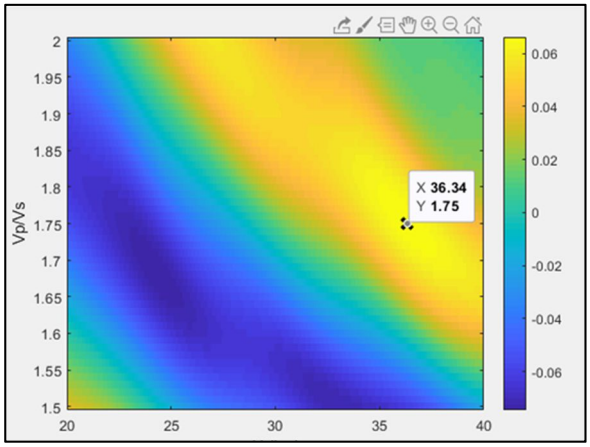

Fig. 28. The results of Moho depth and Vp/Vs velocity using Stacking H-k at MTKI Stations.

4.3 South Borneo Province

In the South Borneo province, there are two seismic stations, namely Kotabaru Station (KBKI) and Banjarbaru Station (BBKI). KBKI Station is located at Latitude -3.29 and Longitude 116.16, situated in the Kotabaru region. This research utilizes 31 receiver functions with a fit value criterion ≥ 90%. The plot of the thirty-one receiver functions for the radial component based on back azimuth and the stacking results can be seen in (Fig. 29). Ps conversion phase is observed at around ~ 5.2 s. Meanwhile, BBKI Station is located at Latitude -3.46 and Longitude 114.84, situated in the Banjar Baru region. In this study, 55 receiver functions are used, and the Ps conversion phase is observed at around ~ 3.8 s. (Figure. 30) shows the results of this research.

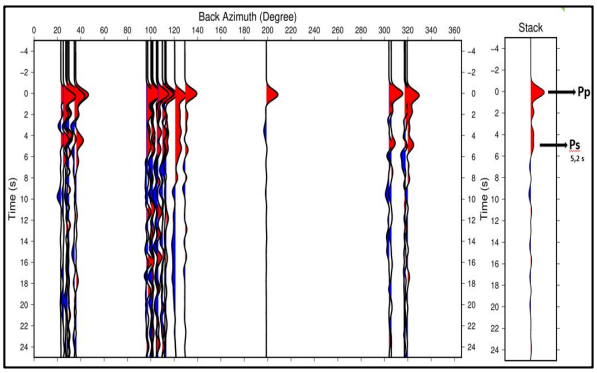

Fig. 29. Receiver function and stacking at KBKI Station plotted based on back azimuth.

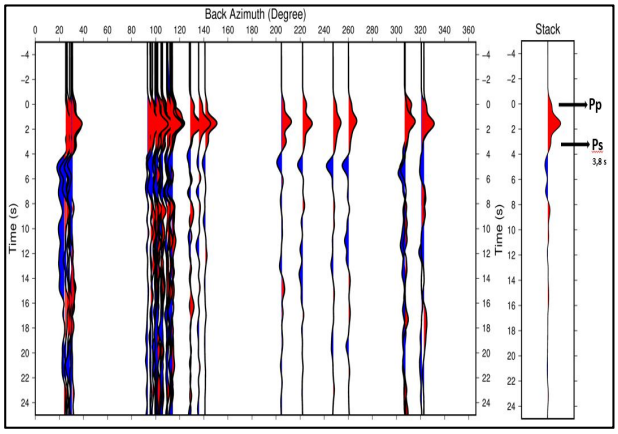

Fig. 30. Receiver function and stacking at BBKI Station plotted based on back azimuth.

The velocity structure of P and S waves beneath KBKI station is depicted through receiver function inversion results using stacked signals. There is a correlation level of 99.03% between the inverted signals and observations beneath KBKI station (Fig. 31). The P-wave velocity profile shows that the range of P-wave velocity from the surface to a depth of 100 km is between 5.8 km/s to 9.8 km/s, with minimum and maximum values. At depths from the surface to 8 km, the velocity increases from around 5.8 km/s to 7.0 km/s. Then, at depths of 9 to 14 km, there is a decrease in velocity to 6.5 km/s to 6.8 km/s. Subsequently, at depths from 15 to 55 km, the velocity rises significantly to approximately 7.4 km/s to 9.8 km/s. Based on this P-wave velocity profile, it is estimated that the depth of the Moho discontinuity layer beneath KBKI station is in the range of 34 to 38 km, with P-wave velocities in the crust ranging from 5.8 km/s to 9.1 km/s (Fig. 32). The results of the S-wave velocity profile show that the range of S-wave velocity from the surface to a depth of 100 km is between 3.2 km/s to 5.5 km/s, with minimum and maximum values (Figure. 33). At depths from the surface to 8 km, the velocity increases from around 3.2 km/s to 3.9 km/s. Then, at depths of 9 to 14 km, there is a decrease in velocity to 3.6 km/s to 3.7 km/s. Subsequently, at depths from 15 to 55 km, the velocity rises significantly to approximately 4.1 km/s to 5.5 km/s. Based on this S-wave velocity profile, S-wave velocities in the crust range from 3.2 km/s to 5.1 km/s.

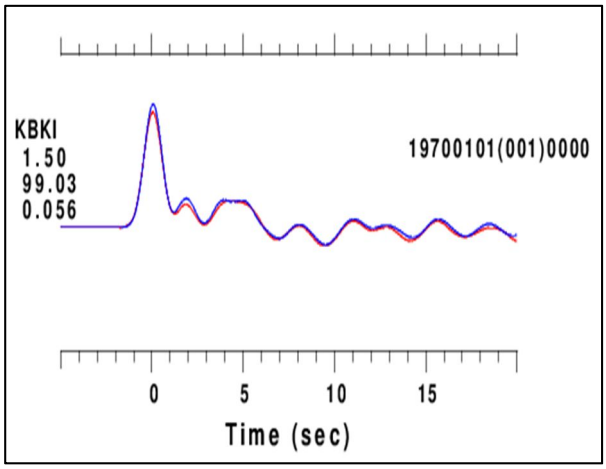

Fig. 31. Comparison of inversion results (red) and observations (blue) from receiver function stacking signals at KBKI Station.

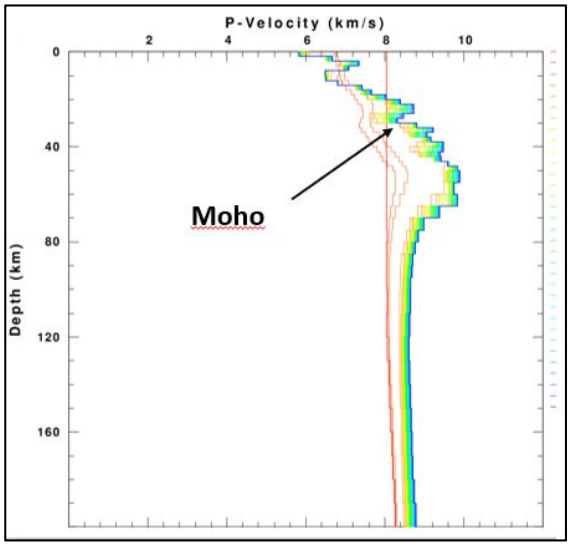

Fig. 32. Profile of P-wave velocity at KBKI Station.

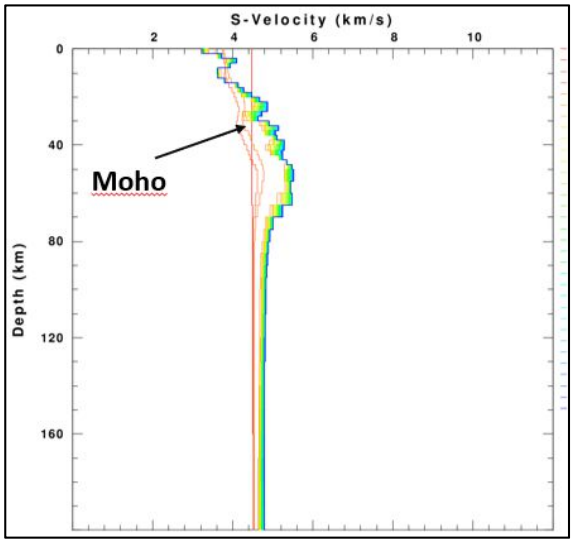

Fig. 33. Profile of S-wave velocity at KBKI Station.

The inversion results of the receiver function at the BBKI station are used to depict the structure of P and S wave velocity. The inverted signals are the outcome of the stacking process. In (Figure. 34), there is an 88.12% match between the inverted signals and the observations beneath the BBKI station. The P-wave velocity profile beneath the BBKI station shows that the velocity range of P waves from the surface to a depth of 100 km is between 2.1 km/s and 9.3 km/s, with the minimum and maximum values. From the surface to a depth of 26 km, the velocity increases from 2.1 km/s to 8.0 km/s. However, at depths of 27 to 80 km, there is a significant decrease in velocity, ranging from 7.7 km/s to 9.3 km/s. This significant decrease is due to the presence of sediment layers causing differences in denser materials. Based on the P-wave velocity profile, it is estimated that the depth of the Moho discontinuity layer beneath the BBKI station is in the range of 26 - 32 km, with P-wave velocities in the crust ranging from 2.1 km/s to 8.0 km/s (Figure. 35). Meanwhile, the S-wave velocity profile beneath the BBKI station indicates that the velocity range of S waves from the surface to a depth of 100 km is between 1.1 km/s and 5.1 km/s, with the minimum and maximum values (Figure. 36). From the surface to a depth of 26 km, the S-

wave velocity increases from 1.1 km/s to 4.4 km/s. However, at depths of 27 to 80 km, there is a significant decrease in velocity, ranging from 5.3 km/s to 5.1 km/s. Based on the S-wave velocity profile, the S-wave velocities in the crust range from 1.1 km/s to 4.4 km/s.

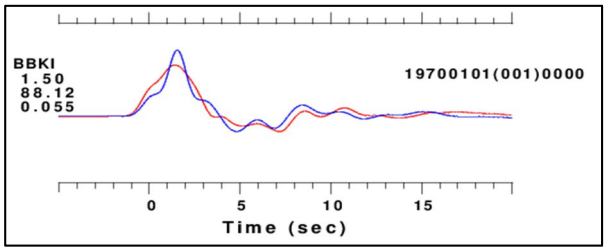

Fig. 34. Comparison of inversion results (red) and observations (blue) from receiver function stacking signals at BBKI Station.

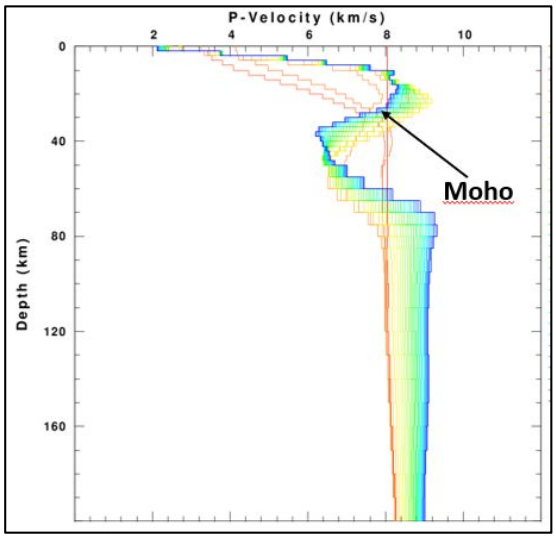

Fig. 35. Profile of P-wave velocity at BBKI Station.

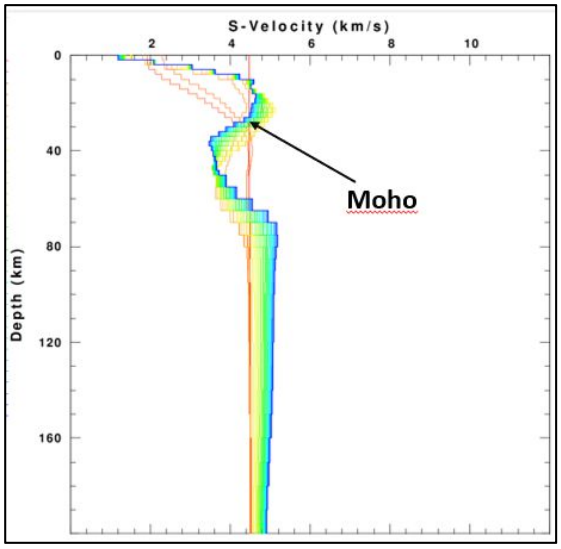

Fig. 36. Profile of S-wave velocity at BBKI Station.

The migration results using the AK-135 velocity model indicate that the depth of the Mohorovicic discontinuity layer beneath KBKI Station is approximately 38 km (Figure. 37), while beneath BBKI Station, it is at a depth of about 26 km. Additionally, at this station, the depth of the basement is also identified to be around 14 km (Figure. 38).

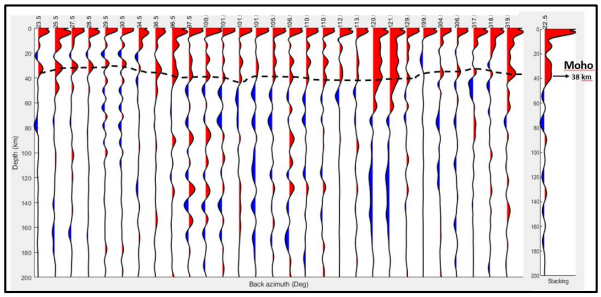

Fig. 37. The migration results using the AK-135 velocity model at KBKI Station.

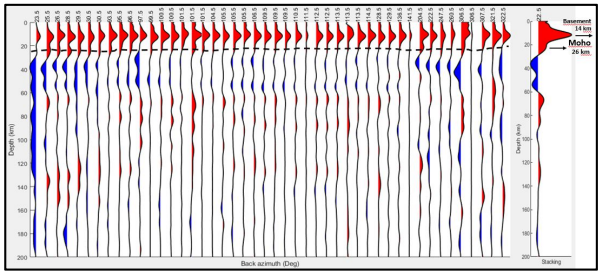

Fig. 38. The migration results using the AK-135 velocity model at BBKI Station.

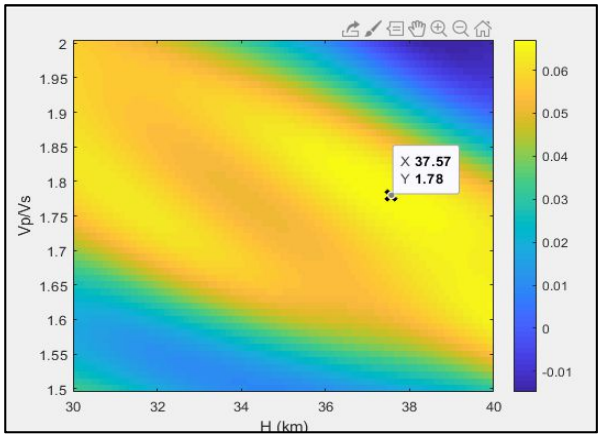

Fig. 39. The results of Moho depth and Vp/Vs velocity using Stacking H-k at KBKI Stations.

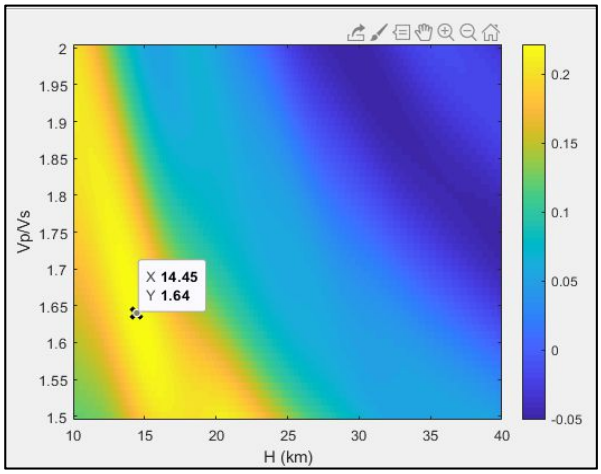

Fig. 40. The results of sediment depth and Vp/Vs velocity using Stacking H-k at BBKI Stations.

Using the H-k Stacking method, the estimation results for the depth of the Mohorovičić discontinuity layer beneath Station KBKI are approximately ~37.57 km, with a Vp/Vs velocity value of 1.78 km/s (Fig. 39). However,

the H-k Stacking results at Station BBKI could not identify the Moho because there is a relatively thick sediment layer beneath the Barito Basin, which is located at a depth of ~14.45 km (Fig. 40).

Based on the results from several stations, the depth of the Moho boundary is shown in (Fig 41). And the detailed results of this research are presented in Table 1.

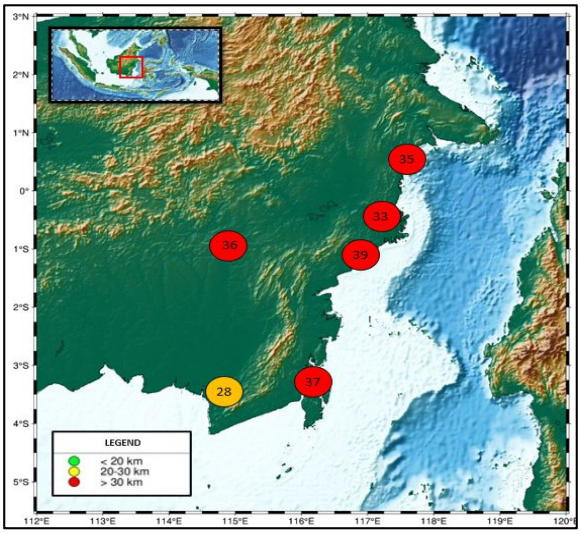

Fig. 41. Distribution of Moho depth beneath each seismic station

Table 1. The result of the identification of the crust around the new capital city area of Indonesia.

Seismic Stations	Earth's Crust			
	Crust Thickness (km)	Vp (km/s)	Vs (km/s)	Vp/Vs (km/s)
SGKI	30 - 40	3.0 - 7.7	1.7 - 3.2	1.96
SMKI	28 - 33	3.7 - 7.7	2.0 - 4.3	1.81
BKB	35 - 43	1.8 - 7.7	1.0 - 4.3	1.97
MTKI	32 - 36	3.7 - 8.0	2.0 - 4.4	1.75
KBKI	34 - 38	5.8 - 9.1	3.2 - 5.1	1.78
BBKI	26 - 32	2.1 - 8.0	1.1 - 4.4	1.64

5 Conclusions

Depth of the Moho boundary layer in East Borneo province at the SGKI station is approximately 30 - 40 km, at the SMKI station is around 28 - 33 km. At the BKB station, it is about 35 - 43 km. Moving on to Central Borneo province, specifically at the MTKI station, the depth is around 32 - 36 km. In South Borneo province, at the KBKI station, the Moho boundary layer is located at a depth of about 34 - 38 km, and at the BBKI station, it is approximately 26 - 32 km.

The P-wave velocity to a depth of 100 km is as follows: In East Borneo province, at the SGKI station, the P-wave velocity is approximately 3.0 – 10.2 km/s, at the SMKI station, it is around 3.7 – 9.1 km/s, and at the BKB station, it is about 1.8 – 9.8 km/s. Moving on to Central Borneo province, specifically at the MTKI station, the P-wave velocity is around 3.7 – 9.2 km/s. In South Borneo province, at the KBKI station, the P-wave velocity ranges from 5.8 – 9.8 km/s, and at the BBKI station, it is approximately 2.1 – 9.3 km/s. The S-wave velocity to a depth of 100 km is as follows: In East Borneo province, at the SGKI station, the S-wave velocity is approximately 1.7 – 5.7 km/s, at the SMKI station, it is around 2.0 - 5.1 km/s, and at the BKB station, it is about 1.0 – 5.4 km/s. Moving on to Central Borneo province, specifically at the MTKI station, the S-wave velocity is around 2.0 – 5.1 km/s. In South Borneo province, at the KBKI station, the S-wave velocity ranges from 3.2 – 5.5 km/s, and at the BBKI station, it is approximately 1.1 – 5.1 km/s.

The author would like to express gratitude to BMKG (Meteorology, Climatology, and Geophysics Agency), the professors, and friends in the Geophysics department who have provided support for this research and UP2KM STMKG (State College of Meteorology Climatology and Geophysics) for funding the publication of this study. Additionally, the author would also like to thank Prof. Robert B Hermann for providing the "Computer Programs in Seismology" software and all other parties involved who have supported this research.

References

1 W. Hamilton, Bull. Geol. Soc. Malaysia, **6**, 3–10, (1973)
2 R. Hall, J. Asian Earth Sci., **20**, 4, 353–431, (2002)
3 S. J. Moss and J. L. C. Chambers, J. Asian Earth Sci., **17**, 1–2, 157–181
4 BPS, Indonesian Population Profile 2015 Supas Results. (2016). (In Indonesia)
5 Law of Indonesia No.3 2022[Online]. Available: https://peraturan.bpk.go.id/Home/Details/198400/uu-no-3-tahun-2022
6 L. Zhu and H. Kanamori, J. Geophys. Res. Solid Earth, **105**, B2, 2969–2980, (2000)
7 T. Lay and T. C. Wallace, Modern Global Seismology (International Geophysics Series, **58**, 58**.** (1995).
8 T. Saita, D. Suetsugu, T. Ohtaki, H. Takenaka, K. Kanjo, and I. Purwana, Geophys. Res. Lett., **29**, 7, 19-1-19–4 (2002)
9 W. Suryanto, B. Nurdiyanto, and S. Pakpahan, J. Meteorol. dan Geofis., **11**, 1, (2010)
10 K. Kieling, D. Rössler, and F. Krüger, J. Seismol., **15**, 2,. 235–259, (2011)
11 S. Bahri, W. Suryanto, and D. Ngadmanto, J. Phys. Conf. Ser., **1825**, 1, 8–14. (2021)
12 S. Syuhada et al., Acta Geophys., 0123456789, (2022)
13 J. P. Ligorría and C. J. Ammon, Bull. Seismol. Soc. Am., **89**, 5, 1395–1 (1999)
14 M. S. Puji Ariyanto, B. Pranata, and B. S. Prayitno, **07**, 03, (2021).
15 J. Julià, C. J. Ammon, R. B. Herrmann, and A. M. Correig, Geophys. J. Int., **143**, 1, 99–112, (2000)
16 B. L. N. Kennett, E. R. Engdahl, and R. Buland, Geophys. J. Int., **122**, 1, 108–124, (1995)
17 W. M. Telford, Nature, **127**, 3212. 783–785. (1990)
18 R. B. Herrmann, **2013**, 1–30, (2009)